Nuclear Instruments and Methods in Physics Research B 505 (2021) 58–63

Contents lists available at ScienceDirect

Nuclear Inst. and Methods in Physics Research, B

journal homepage: www.elsevier.com/locate/nimb

Effect of hydrogen implantation on low-temperature activation of boron in silicon

Jui-Chang Lin [a], Bo-Wen Lee [a], Ruey-Dar Chang [a,*], Che-Men Chu [b], Wei-Yen Woon [b]

[a] Department of Electronics Engineering, Chang Gung University, 259 Wenhua 1st Road, Guishan, Taoyuan 33302, Taiwan, ROC
[b] Department of Physics, National Central University, 300 Zhongda Road, Zhongli, Taoyuan 32001, Taiwan, ROC

ARTICLE INFO

Keywords:
Boron
Ion implantation
Hydrogen
Activation
Defect

ABSTRACT

Understanding the behavior of dopant activation at low temperatures is necessary for three-dimensional integration of transistors. In this work, the impact of hydrogen coimplantation on boron activation was investigated at implantation doses below the amorphization threshold. The carrier depletion effect due to substrate doping was simulated to accurately characterize the initial activation behavior of boron. At temperatures higher than 400 °C, the boron activation level decreased as the hydrogen dose increased. The deactivation caused by hydrogen diminished after extended annealing at 500 °C. This indicated the passivation of boron by hydrogen. However, the boron activation in the sample implanted with hydrogen at a dose of 1×10^{15} cm^{-2} was first degraded and then enhanced during annealing at 300 °C. The time-dependent activation behavior suggested the elimination of isolated defects via reactions associated with hydrogen migration.

1. Introduction

Ion implantation has long been used to introduce dopants in integrated circuits at low temperatures to locally modify transistor characteristics. The density of transistors in integrated circuits can be increased by vertically stacking transistors. Stacked thin-film transistors (TFTs) were used to decrease the cell size of static random-access memory [1]. Nonplanar polycrystalline silicon TFTs were vertically integrated to fabricate three-dimensional NAND flash memory [2]. The low-temperature activation of implanted dopants is required for three-dimensional process integration. Conventionally, dopants can be activated via the recrystallization of amorphized silicon. However, it was reported that recrystallization in fin structures promoted nucleation of polycrystalline silicon owing to the formation of twin boundaries [3]. Therefore, amorphization is not suitable for nonplanar device structures. Only a few studies have investigated dopant activation under subamorphizing implantation at low temperatures [4–7]. Formation of a vacancy-rich region via silicon implantation was shown to improve boron activation at low temperatures [7]. Since defect accumulation should be reduced to prevent amorphization in nonplanar device structures, hydrogen implantation has the potential to be used for point-defect engineering. It was reported that hydrogen enhanced boron activation at low temperatures when the sheet resistivity or spreading resistance profiling was used for activation analysis [8,9]. However, the capacitance–voltage curves of metal–oxidesemiconductor capacitors or Schottky diodes demonstrated the deactivation of acceptors owing to hydrogen [10–12]. The analysis techniques and process conditions for sample preparation used in these studies were quite different. Therefore, the role of hydrogen in boron activation must be examined further. In this work, the subamorphizing implantation of boron was performed in conjunction with device simulation to study the activation behavior at low temperatures. The degradation and enhancement of boron activation due to hydrogen implantation was observed depending on the hydrogen dose and annealing temperature.

2. Experimental method

(100) n-type silicon wafers were oxidized to form a cap oxide layer with a thickness of 50 nm. The cap oxide was used as a mask to form the device structure for Hall measurements based on the van der Pauw method. The structure and process conditions of the test device are described in our previous paper [13]. In this study, boron atoms were implanted into the central device region at 30 keV and a dose of 5×10^{13} cm^{-2}. Then hydrogen implantation was performed at 7 keV and doses of 10^{13}–10^{15} cm^{-2}. Boron and hydrogen were implanted at a tilt angle of 7°. Fig. 1 shows the Monte Carlo simulation [14] result for the

* Corresponding author.
E-mail address: crd@mail.cgu.edu.tw (R.-D. Chang).

https://doi.org/10.1016/j.nimb.2021.08.009
Received 21 June 2021; Received in revised form 27 August 2021; Accepted 30 August 2021
Available online 11 September 2021

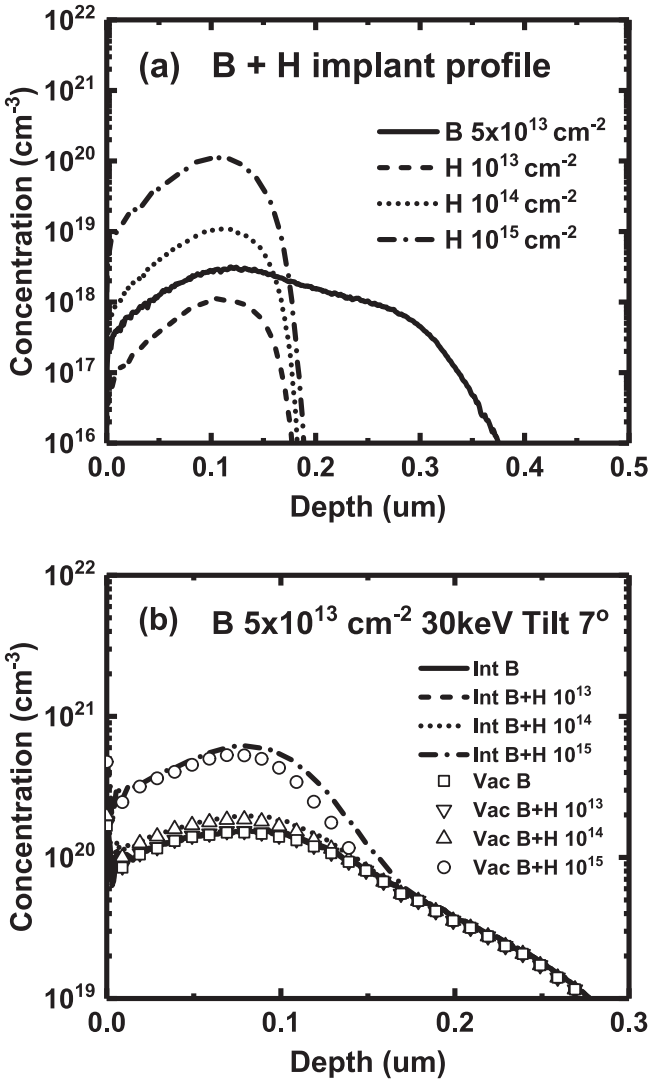

Fig. 1. Boron and hydrogen implantation profiles obtained from Monte Carlo simulation. The distributions of generated point defects are also shown.

coimplantation of boron and hydrogen. Damage accumulation and dynamic annealing were considered in the simulation. Since the experimental conditions were chosen to reduce defect accumulation, complex reactions between defects rarely occurred during ion implantation. The impact of defect recombination on the calculation of defect concentrations was limited. Ion channeling caused a secondary peak of boron near the bulk. Implantation might produce defect states affecting the electrical measurements. Therefore, the profiles of the point defects generated by hydrogen implantation were located away from the junction. The peak profiles of hydrogen were close to that of boron. Fig. 1 shows the distribution of point defects generated by boron and hydrogen implantation. The peak concentration of point defects in the samples with hydrogen coimplantation at a dose of 10^{15} cm^{-2} was approximately four times larger than that in the sample with only boron implantation. The concentration of point defects increased by approximately 30% when hydrogen was implanted at a dose of 10^{14} cm^{-2} after boron implantation. No evident difference was observed between the point defect profiles in the samples with and without hydrogen coimplantation at a dose of 10^{13} cm^{-2}. The implanted samples were subsequently cycled between rapid thermal annealing (RTA) and Hall measurements to monitor the time evolution of boron activation. A Hall scattering factor of 0.8 was adopted to obtain the sheet concentration of holes [15].

3. Results and discussion

Fig. 2 shows the measurement result for the samples with and without hydrogen implantation during RTA at 300 °C. The sheet resistance decayed with time, indicating the activation of implanted boron. The sample with hydrogen coimplantation at a high dose of 1×10^{15} cm^{-2} exhibited the highest sheet resistance at the beginning of annealing. It is interesting to note that the sheet resistance of the sample became the lowest as the annealing time increased. The sheet resistance of the other hydrogen-implanted samples was always higher than that of the sample implanted only with boron. The time evolution of the sheet carrier concentration clearly indicated that the activation rate decreased with time. In the early stage of annealing, the sheet carrier concentration decreased as the hydrogen implantation dose increased. A similar trend was observed during the extended annealing of the samples implanted with hydrogen at doses of 1×10^{13} and 1×10^{14} cm^{-2}. However, the carrier concentration of the sample with hydrogen implantation at a dose of 1×10^{15} cm^{-2} exceeded that of the sample without hydrogen implantation as the annealing time increased. The Hall mobility did not change significantly during annealing. The sample with hydrogen implantation at a dose of 1×10^{15} cm^{-2} exhibited a higher mobility at the beginning of annealing. This was possibly due to the low active boron concentration which caused less carrier scattering. However, the mobility remained high, even though boron activation was considerably improved. This implies that hydrogen might passivate defects to reduce carrier scattering.

Fig. 3 presents the activation behavior during annealing at 400 °C for the samples with and without hydrogen implantation. The sample with hydrogen implantation at a dose of 1×10^{15} cm^{-2} exhibited a high sheet resistance for all annealing times. In other samples, as the annealing time increased, the sheet resistance first decreased and then became stable. The corresponding sheet carrier concentration demonstrated the saturation of boron activation following a decline of the activation rate. Although the Hall mobility slightly increased with the hydrogen implantation dose, a severe degradation of boron activation was observed in hydrogen-implanted samples. The saturation level of the sheet carrier concentration was suppressed as more hydrogen atoms were implanted into the substrate.

Fig. 4 demonstrates the impact of hydrogen implantation on boron activation during annealing at 500 °C. Boron activation was suppressed owing to hydrogen implantation in the early stage of annealing. However, as the annealing time increased, the curves of the sheet resistance and carrier concentration for the samples with hydrogen implantation converged to those for the samples without hydrogen implantation. A similar convergence trend was observed for the Hall mobility. The disappearance of the hydrogen effect implies that the outdiffusion of hydrogen might occur during extended annealing at 500 °C.

The distribution of carriers might not be the same as that of the dopants in the test device. Therefore, a two-dimensional device simulation [16] was carried out to verify the effect of carrier redistribution in the test structure. The potential at the silicon surface was not assigned except at two contact corners. The carrier redistribution along the current conduction path was neglected because a low bias was applied during the measurements. The boron implantation profile was scaled to approximate the acceptor profiles for different activation levels. The corresponding hole distribution was obtained by performing a device simulation for each acceptor profile. Fig. 5 compares the simulation results for different activation levels. An evident discrepancy was observed between the hole and acceptor profiles for boron activation at a dose of 1.3×10^{11} cm^{-2}. The peak of the hole profile shifted to the surface, and the concentration of holes was significantly lower than that of the acceptors. This implied that the depletion region was extended toward the surface. The depletion region close to the p-n junction created a barrier to isolate the conducting holes from the substrate. The isolation is necessary for performing Hall measurements; otherwise, the electron conduction in the n-type substrate would affect the measured

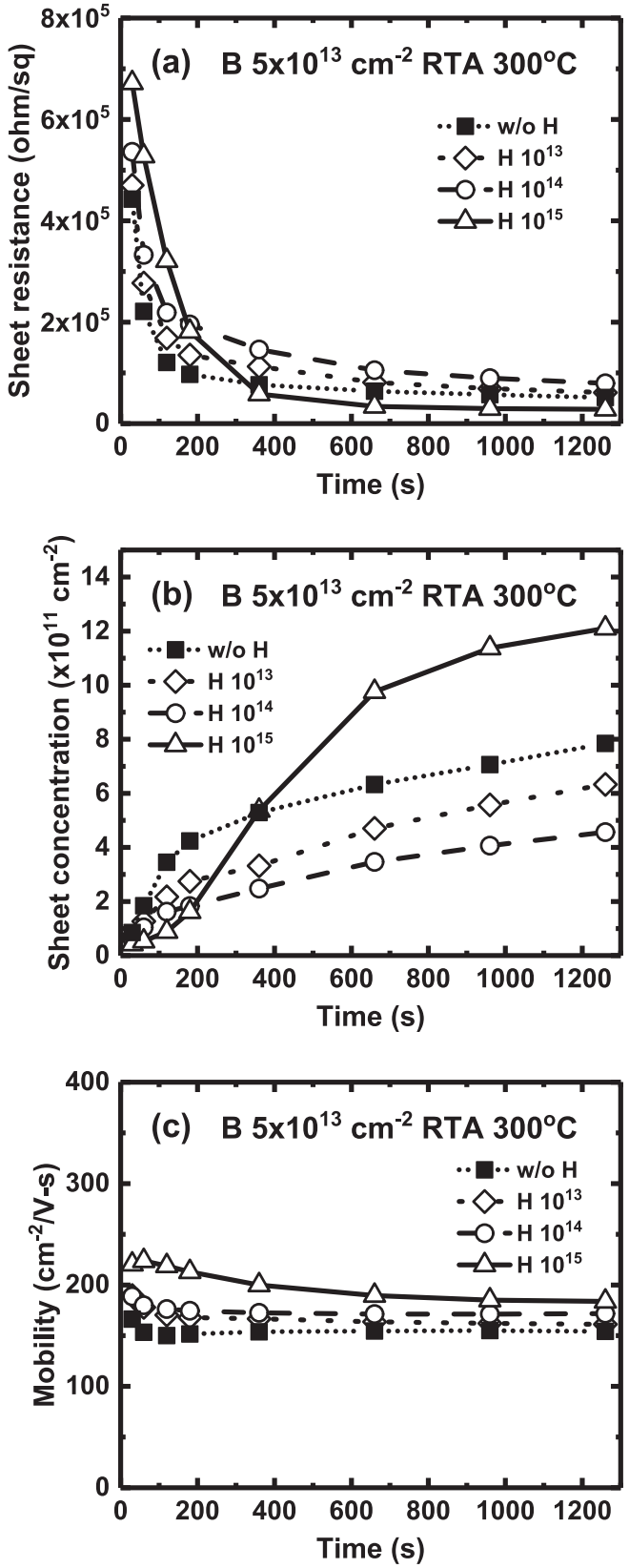

Fig. 2. (a) Sheet resistance, (b) sheet carrier concentration, and (c) Hall mobility in samples implanted with boron at a dose of 5×10^{13} cm^{-2} with and without hydrogen during RTA at 300 °C.

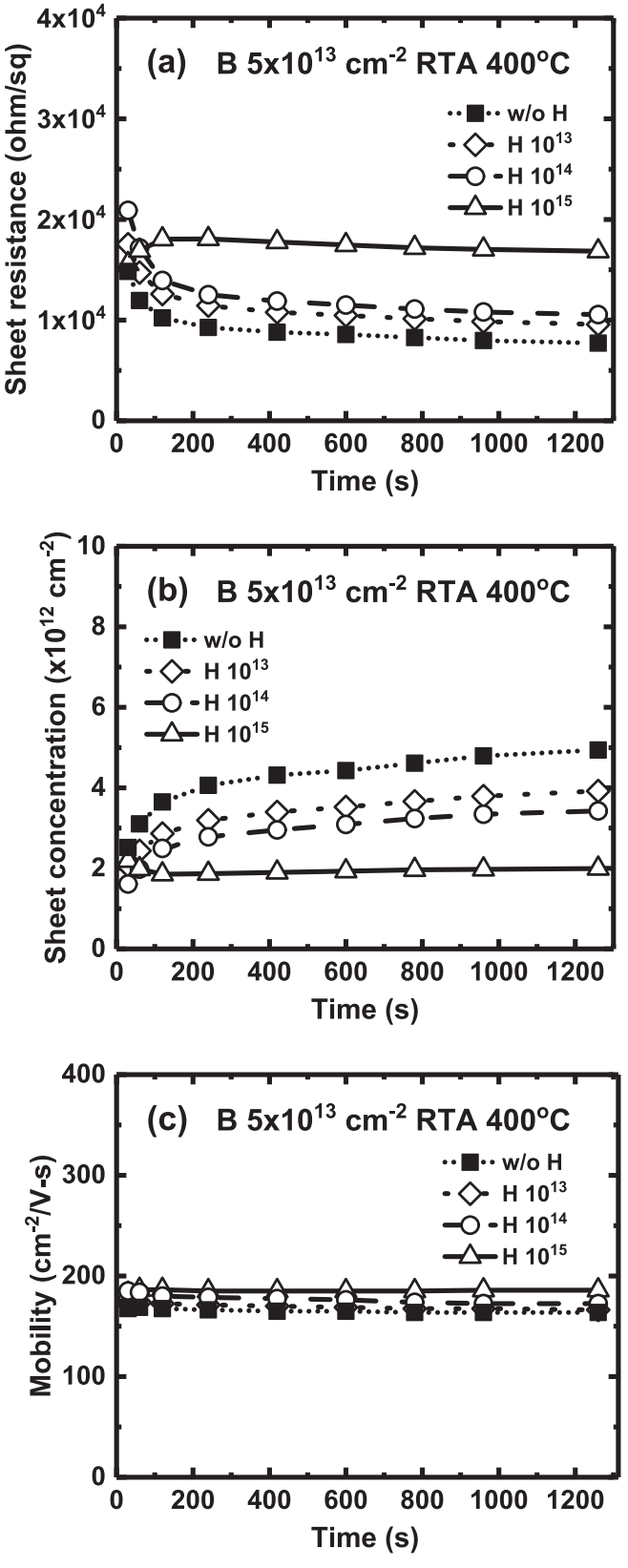

Fig. 3. (a) Sheet resistance, (b) sheet carrier concentration, and (c) Hall mobility for boron-implanted samples with and without hydrogen implantation during RTA at 400 °C.

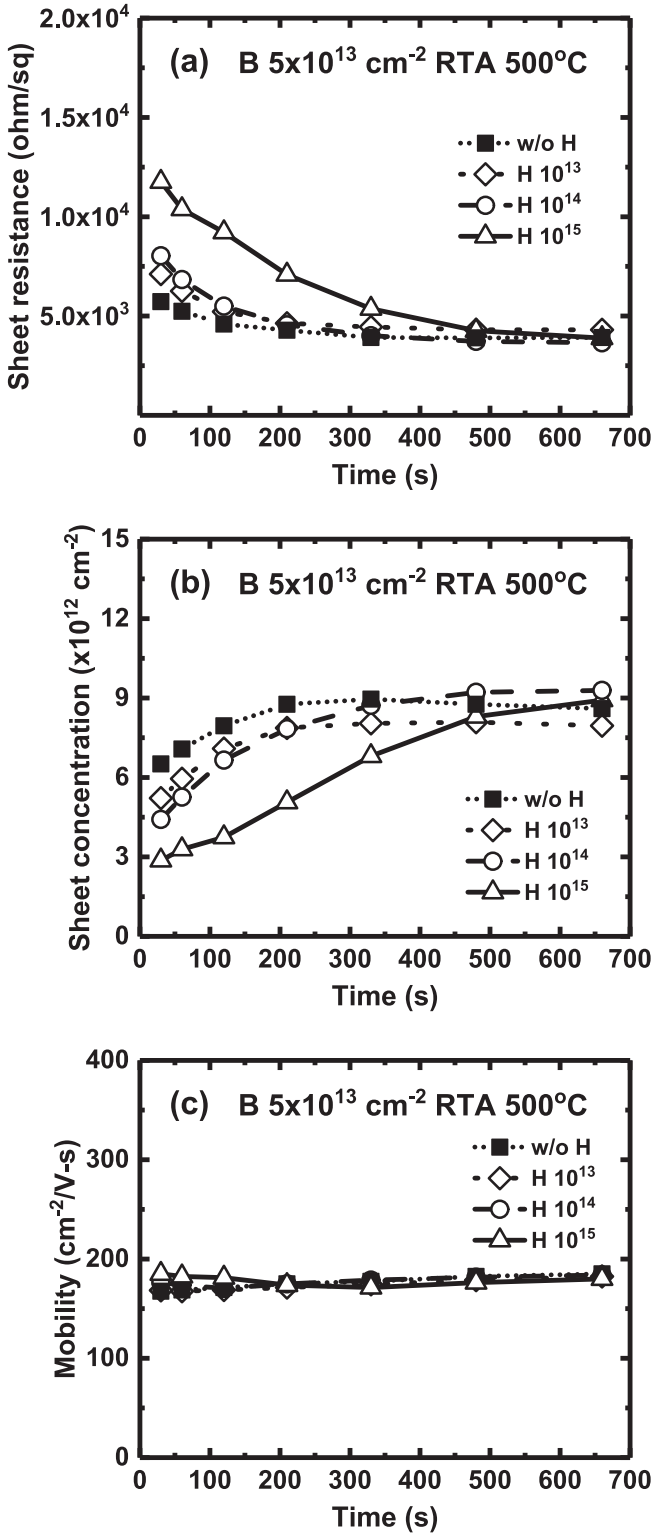

Fig. 4. Time evolution of (a) sheet resistance, (b) sheet carrier concentration, and (c) Hall mobility in boron-implanted samples with different hydrogen doses during RTA at 500 °C.

Hall potential. A large fraction of holes was depleted when a few acceptors were ionized. This shifted the hole profile and reduced the sheet carrier concentration. When the active boron dose was increased to 5×10^{13} cm^{-2}, the number of depleted holes remained similar. The impact of the depletion effect on the carrier distribution became small. As a result, the difference between the hole and acceptor profiles was not

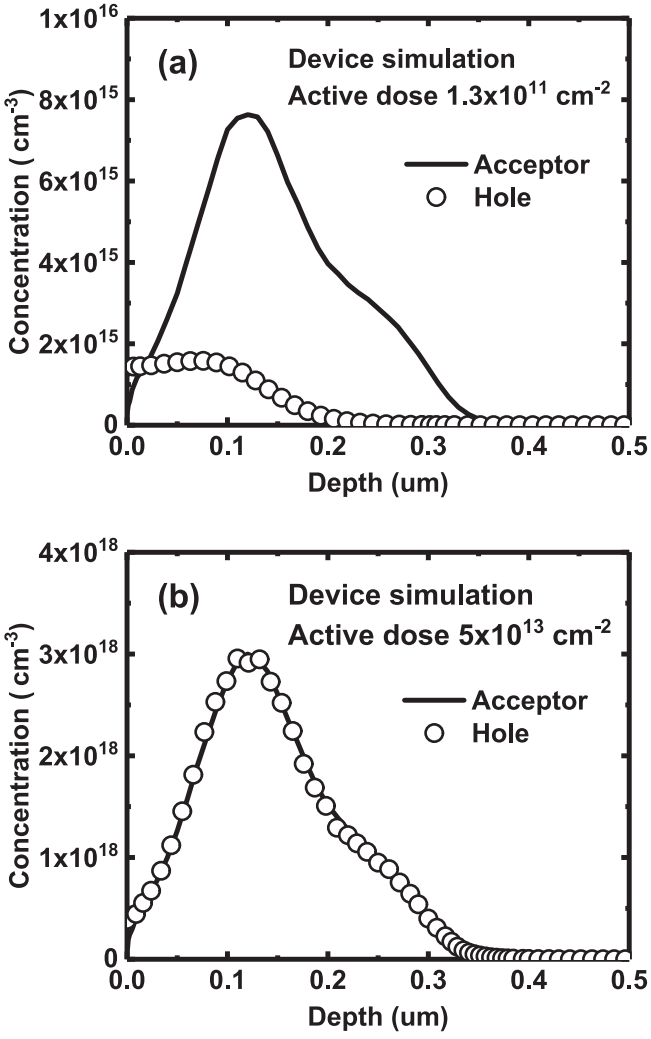

Fig. 5. Hole profiles obtained from device simulation at active boron doses of (a) 1.3×10^{11} and (b) 5×10^{13} cm^{-2}.

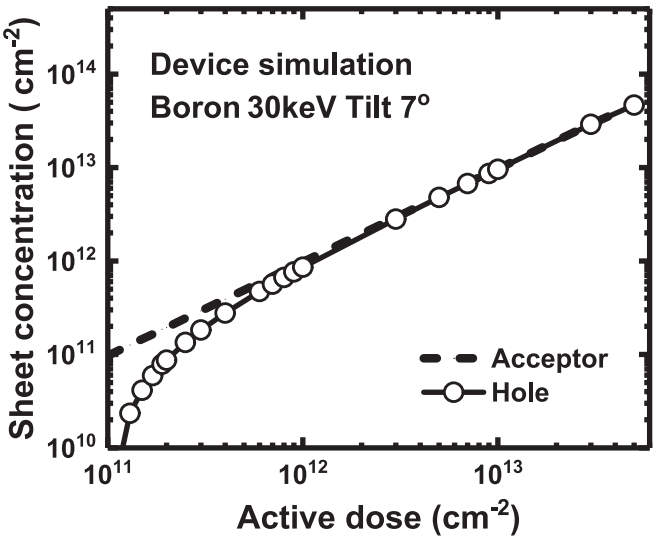

Fig. 6. Comparison of the active boron dose and sheet carrier concentration for different activation levels.

evident.

Fig. 6 shows the sheet carrier concentration of holes as a function of the active boron dose obtained using device simulation. The sheet carrier concentration was almost identical to the active dose when the activation level was over 2×10^{12} cm^{-2}. The sheet carrier concentration was considerably less than the active dose when the active level was approximately 10^{11} cm^{-2}. Therefore, the Hall measurement result was corrected on the basis of the device simulation result for the initial activation behavior of boron. The measured sheet carrier concentration was converted to the active boron dose via linear interpolation using the curves in Fig. 6. Fig. 7 shows the active boron dose after the aforementioned correction. The initial activation rate at 300 °C was higher than that estimated by the sheet carrier concentration from the Hall measurement. For activation at 400 and 500 °C, the active boron dose was similar to the sheet carrier concentration after the correction because the carrier depletion effect could be neglected at high activation levels.

Hydrogen implantation evidently affected on boron activation. At 300 °C, boron activation was degraded in the samples with hydrogen implantation at the beginning of annealing. However, boron activation was enhanced in the samples with hydrogen implantation at a dose of 1×10^{15} cm^{-2} as the annealing time increased. The saturation level of active boron decreased with the hydrogen dose during annealing at 400 °C. The degradation of activation caused by hydrogen diminished at 500 °C after extended annealing. The annealing of compensating defects was proposed to explain the dopant activation behavior [17]. However, boron activation tended to become saturated after extended annealing. This implied the formation of metastable defect complexes which delayed the defect annealing process. The boron activation in the early stage of RTA was mainly due to the annihilation of isolated point defects. The point defect profiles in Fig. 1 showed that hydrogen implantation at a dose of 1×10^{15} cm^{-2} caused extensive damage. The impact of this damage on boron activation cannot be neglected [18,19]. However, the point defect profiles for the sample implanted with hydrogen at 1×10^{13} cm^{-2} were the same as those for the sample without hydrogen implantation. Thus, the deactivation in the sample was mainly caused by hydrogen atoms. Several mechanisms were proposed to explain the passivation of acceptors by hydrogen [20–22]. Our result indicated that the degree of boron deactivation was not proportional to the hydrogen implantation dose. The hydrogen passivation effect observed in this study is not likely to be caused by the direct interaction between boron and hydrogen atoms. The decrease in the passivation effect during extended annealing at 500 °C is possibly due to dehydrogenation [10]. During the annealing of the sample with hydrogen implantation at 1×10^{15} cm^{-2}, the activation behavior at 300 °C was first degraded and then enhanced as the annealing time increased. This is possibly related to the migration of hydrogen atoms. The creation of vacancies due to hydrogen diffusion was proposed as a mechanism for enhanced activation [8]. This implies that point defect reactions might improve the annihilation of isolated defects, leading to enhanced activation at 300 °C. However, the reactions did not enhance the annihilation of metastable defect complexes, which determined the saturation of boron activation at 400 °C. Thus, the hydrogen passivation effect dominated the activation at 400 °C, causing boron deactivation. Since the implantation dose of boron was not high in this study, the passivation of boron due to hydrogen did not greatly affect the mobility of holes. The Hall mobility slightly increased with the hydrogen implantation at a dose of 1×10^{15} cm^{-2}.

4. Conclusions

The subamorphizing implantation of boron and hydrogen was performed to investigate the impact of hydrogen on boron activation at temperatures of 300–500 °C. As holes may be depleted by donors in the substrates, a device simulation was performed to correct the active boron dose after Hall measurements. Boron activation was evidently

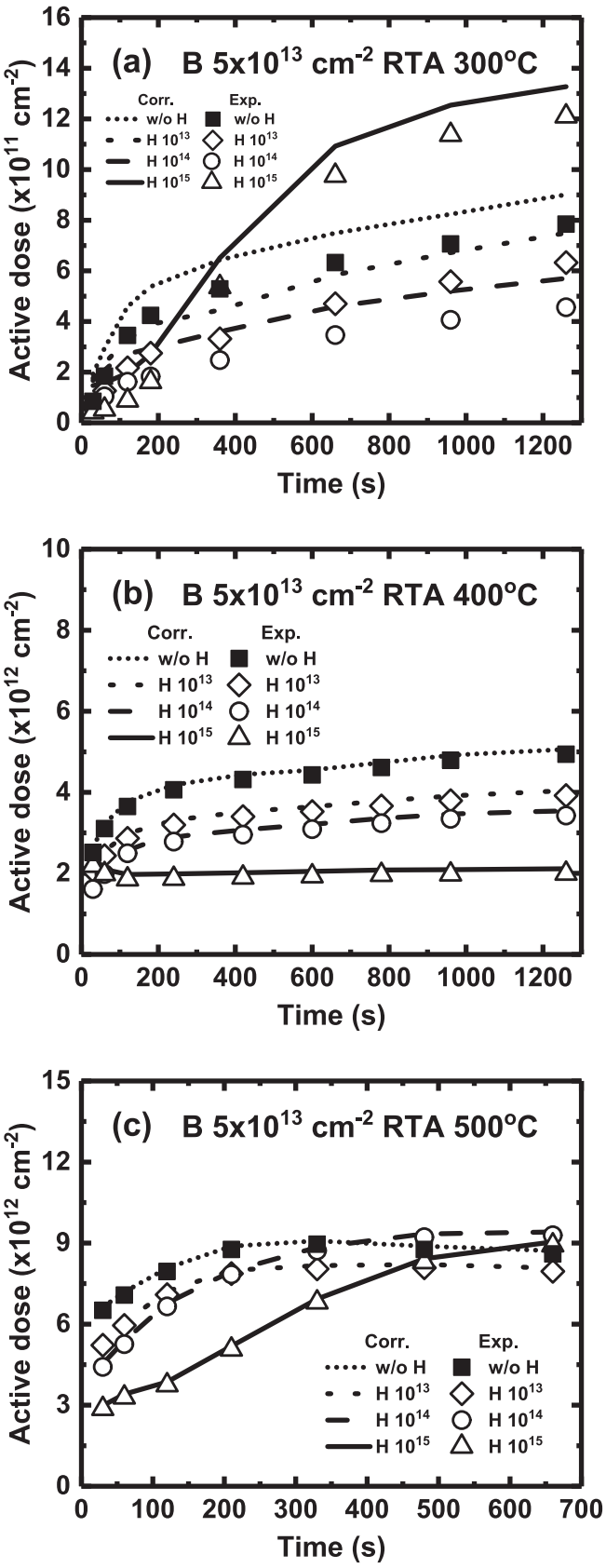

Fig. 7. Active boron dose after correction of the experimental result by device simulation.

degraded in the samples with hydrogen implantation at a dose of 1×10^{13} cm^{-2} at all temperatures, even though the point defect profiles in the samples with and without hydrogen implantation were similar. This implied that the deactivation was mainly caused by hydrogen passivation, which diminished during extended annealing at 500 °C. However, for the sample implanted by hydrogen at a dose of 1×10^{15} cm^{-2}, the activation behavior was first degraded and then enhanced during annealing at 300 °C. This implies that hydrogen migration might induce point defect reactions, which enhance boron activation by eliminating isolated defects.

CRediT authorship contribution statement

Jui-Chang Lin: Investigation, Data curation, Visualization. **Bo-Wen Lee:** Investigation, Data curation. **Ruey-Dar Chang:** Conceptualization, Methodology, Investigation, Writing - review & editing, Supervision. **Che-Men Chu:** Data curation. **Wei-Yen Woon:** .

Declaration of Competing Interest

The authors declare the following financial interests/personal relationships which may be considered as potential competing interests: Authors Jui-Chang Lin, Bo-Wen Lee, and Ruey-Dar Chang receive research support from the Ministry of Science and Technology of the Republic of China, Taiwan, under Contract No. MOST-109-2221-E-182-023; Authors Che-Men Chu and Wei-Yen Woon receive research support from the Ministry of Science and Technology of the Republic of China, Taiwan, under Contract No. MOST-109-2628-M-008 -004 -MY3.

Acknowledgements

The authors would like to thank the Ministry of Science and Technology of the Republic of China, Taiwan, for financially supporting this work under Grants MOST-109-2221-E-182-023 and MOST-109-2628-M-008 -004 -MY3.

References

[1] S. Ikeda, S. Hashiba, I. Kuramoto, H. Katoh, S. Ariga, T. Yamanaka, T. Hashimoto, N. Hashimoto, S. Meguro, Proc. Int. Electron Dev. Meet. (1990) 469–472.
[2] J. Jang, H. S. Kim, W. Cho, H. Cho, J. Kim, S. I. Shim, Y. Jang, J. H. Jeong, B. K. Son, D. W. Kim, K. Kim, J. J. Shim, J. S. Lim, K. H. Kim, S. Youn Yi, J. Y. Lim, D. Chung, H. C. Moon, S. Hwang, J. W. Lee, Y. H. Son, U. I. Chung, W. S. Lee, in: Proceeding of the Symposium on VLSI Technology, 2009, pp. 192-193.
[3] R. Duffy, M.J.H. Van Dal, B.J. Pawlak, M. Kaiser, R.G.R. Weemaes, B. Degroote, E. Kunnen, E. Altamirano, Appl. Phys. Lett. 90 (2007), 241912.
[4] D.E. Davies, Appl. Phys. Lett. 14 (1969) 227–229.
[5] T. E. Seidel, A. U. Mac Rae, Rad. Eff. 7 (1970) 1-6.
[6] S. Oosterhoff, J. Middelhoek, Solid State Electron. 28 (1985) 427–433.
[7] R. Kalyanaraman, V.C. Venezia, L. Pelaz, T.E. Haynes, H.-J. Gossmann, C. S. Rafferty, Appl. Phys. Lett. 82 (2003) 215–217.
[8] A. Vengurlekar, S. Ashoka, C.E. Kalnas, N.D. Theodore, Appl. Phys. Lett. 82 (2003) 4052–4054.
[9] T. Sameshima, T. Uehara, T. Sugawara, M. Hasumi, T. Nagao, K. Yasuta, Y. Inouchi, J. Tatemichi, Proc. Int. Conf. Ion Implantat. Technol. (2018) 46–49.
[10] J.I. Pankove, D.E. Carlson, J.E. Berkeyheiser, R.O. Wance, Phys. Rev. Lett. 51 (1983) 2224–2225.
[11] C.T. Sah, J.Y.C. Sun, Joseph J. Tzou, Appl. Phys. Lett. 43 (1983) 204–206.
[12] R. Rizk, P. de Mierry, D. Ballutaud, M. Aucouturier, D. Mathiot, Phys. Rev. B 44 (1991) 6141–6151.
[13] R.D. Chang, J.C. Lin, B.W. Lee, Jpn. J. Appl. Phys. 59 (2020), 096501.
[14] Sentaurus Process User Guide, Synopsys, Inc., Mountain View, 2015.
[15] Y. Sasaki, K. Itoh, E. Inoue, S. Kishi, T. Mitsuishi, Solid State Electron. 31 (1988) 5–12.
[16] Medici User Guide, Synopsys, Inc., Mountain View, 2009.
[17] J. C. North, W. M. Gibson, Appl. Phys. Lett. 16 (1970) 126-129. [18].
[18] Z.F. Di, Y.Q. Wang, M. Nastasi, N.D. Theodore, Appl. Phys. Lett. 96 (2010), 154103.
[19] F.-X. Darras, N. Cherkashin, F. Cristiano, E. Scheid, O. Kononchuk, L. Capello, A. Claverie, Nucl. Instrum. Meth. B 327 (2014) 29–32.
[20] J.I. Pankove, P.J. Zanzucchi, C.W. Magee, G. Lucovsky, Appl. Phys. Lett. 46 (1985) 421–423.
[21] S.T. Pantelides, Appl. Phys. Lett. 50 (1987) 995–997.
[22] M. Stavola, S.J. Pearton, J. Lopata, W.C. Dautremont-Smith, Appl. Phys. Lett. 50 (1987) 1086–1088.